Parameter Forecasts From CMB Lensing and Galaxy Lensing Power- and Bispectra

Jonas Frugte[1] and **P. Daniel Meerburg**[2]

[1]Independent Researcher ∞, The Netherlands
[2]Van Swinderen Institute for Particle Physics and Gravity, University of Groningen, Nijenborgh 4, 9747 AG Groningen, The Netherlands

E-mail: jonasfrugte@gmail.com

20 February 2025

Abstract

(Placeholder text written with chatgpt) We present a Fisher forecast analysis of the constraints on cosmological parameters from measurements of CMB lensing and galaxy weak lensing power- and bispectra. Using simulated data consistent with upcoming surveys, we explore the sensitivity of lensing observables to parameters including the Hubble constant H_0, baryon density $\Omega_b h^2$, dark matter density $\Omega_c h^2$, scalar spectral index n_s, amplitude of scalar fluctuations A_s, and the sum of neutrino masses $\sum m_\nu$.

Our results indicate that combining power- and bispectra improves parameter constraints compared to power spectra alone, reducing uncertainties by a factor of $\sim X\%$. In particular, we forecast constraints of $\sigma(H_0) = X.X$ km/s/Mpc, $\sigma(\Omega_b h^2) = X.XXX$, $\sigma(\Omega_c h^2) = X.XXX$, $\sigma(n_s) = X.XXXX$, $\sigma(A_s) = X.XX \times 10^{-9}$, and $\sigma(\sum m_\nu) = X.XX$ eV. These results demonstrate the potential of bispectrum measurements in future surveys such as the Simons Observatory, CMB-S4, LSST, and Euclid.

Additionally, we investigate the impact of different noise models and survey redshift distributions, finding that improvements in galaxy redshift accuracy significantly enhance constraints on $\sum m_\nu$. We also discuss the degeneracies between parameters and assess their impact using eigenvalue analysis of the Fisher matrix.

This study highlights the advantages of combining lensing power- and bispectra for cosmological parameter estimation and provides a roadmap for optimizing future surveys to maximize their scientific return.

1 Introduction

Weak lensing has been used as a probe to constrain cosmological parameters since the 2000's [19, 3, 17, 30, 5]. A range of upcoming surveys, such as the survey by the Simons Observatory (SO) [1], the Legacy Survey of Space and Time (LSST) [15], and Euclid [20] aim to measure weak lensing of the CMB and of galaxies. They will do so much more accurately than previous surveys, enabling tighter constraints on parameters and progressing our understanding of physics as a whole. Typically, the main value of interest is the power spectrum (or equivalently, two point function) of the lensing potential. This can be measured in terms of the lensing convergence κ, lensing shear γ, or lensing potential ψ. In the weak lensing regime they all contain the same amount of information and can be easily converted into one another, see section 3. For the CMB the lensing potential is generally measured directly [25], while with galaxies one instead measures the shear, as this can be deduced from the ellipiticity distribution of the observed galaxies [13].

Even with Gaussian initial conditions, there are significant amounts of non-Gaussianity in the weak lensing signal, especially in galaxy lensing due to it being a probe of the more recent distribution of matter [6, 27]. In addition to looking at the power spectrum, a natural next step is thus to measure the lensing bispectrum. This has already been done for signals from galaxies [31], but no proper detection has been done of the CMB lensing bispectrum. Upcoming surveys such as the ones mentioned earlier may detect this signal. Therefore it is relevant to know the detectability of, and parameter constraints possible from, all 4 signals: CMB lensing power- and bispectra and galaxy lensing power- and bispectra. Notably, this includes looking at cross correlation as well.

In this article we aim to answer this question in the context of experimental parameters similar to those of next generation surveys such as mentioned earlier. We are especially interested in seeing if approximate parameter degeneracies can be broken by combining all data. Calculating the covariance matrix of unbiased optimal estimators of the cosmological parameters can be done by combining cosmological simulations (in our case we use the CAMB package [21]) with a Fisher matrix analysis. See figure 1 for an overview of the calculation done in this paper. The parameters looked at are the Hubble constant, H_0, physical baryon density, $\Omega_b h^2$, physical cold dark matter density, $\Omega_c h^2$, scalar spectral index, n_s, amplitude of primordial scalar fluctuations, A_s, sum of neutrino masses $\sum m_\nu$, and dark energy equation of state parameter, w_0. Though, we will find that some of the parameters are poorly constrained even when combining all 4 signals and thus omit them from the analysis in the results. As a secondary purpose, this paper also includes a derivation for the Fisher matrix formalism in the non-trivial context of bispectra with multiple tracers. The final formula can already be found in the literature (see e.g. the appendix of [18]), but the authors of this paper were not able to find a derivation and hence included it.

The structure of this paper is as follows: we first review the theory of weak lensing and weak lensing statistics in sections 2 and 3. We then provide technical details of the calculation in section 4, such as choices for noise and numerical approximations made in the code. In section 5 we present the results, consisting of signal to noise ratios and parameter constraints for different combinations of the CMB and galaxy lensing power- and bispectra. We conclude in section 6. Appendix A contains a short review of the Fisher matrix formalism and gives a technical derivation of the formula used to calculate each Fisher matrix element in the case of bispectra measurements with multiple tracers. Finally, appendix B explains how to relate the shear to the lensing potential in spherical harmonic space.

All code written for this project is uploaded on github at LINK .

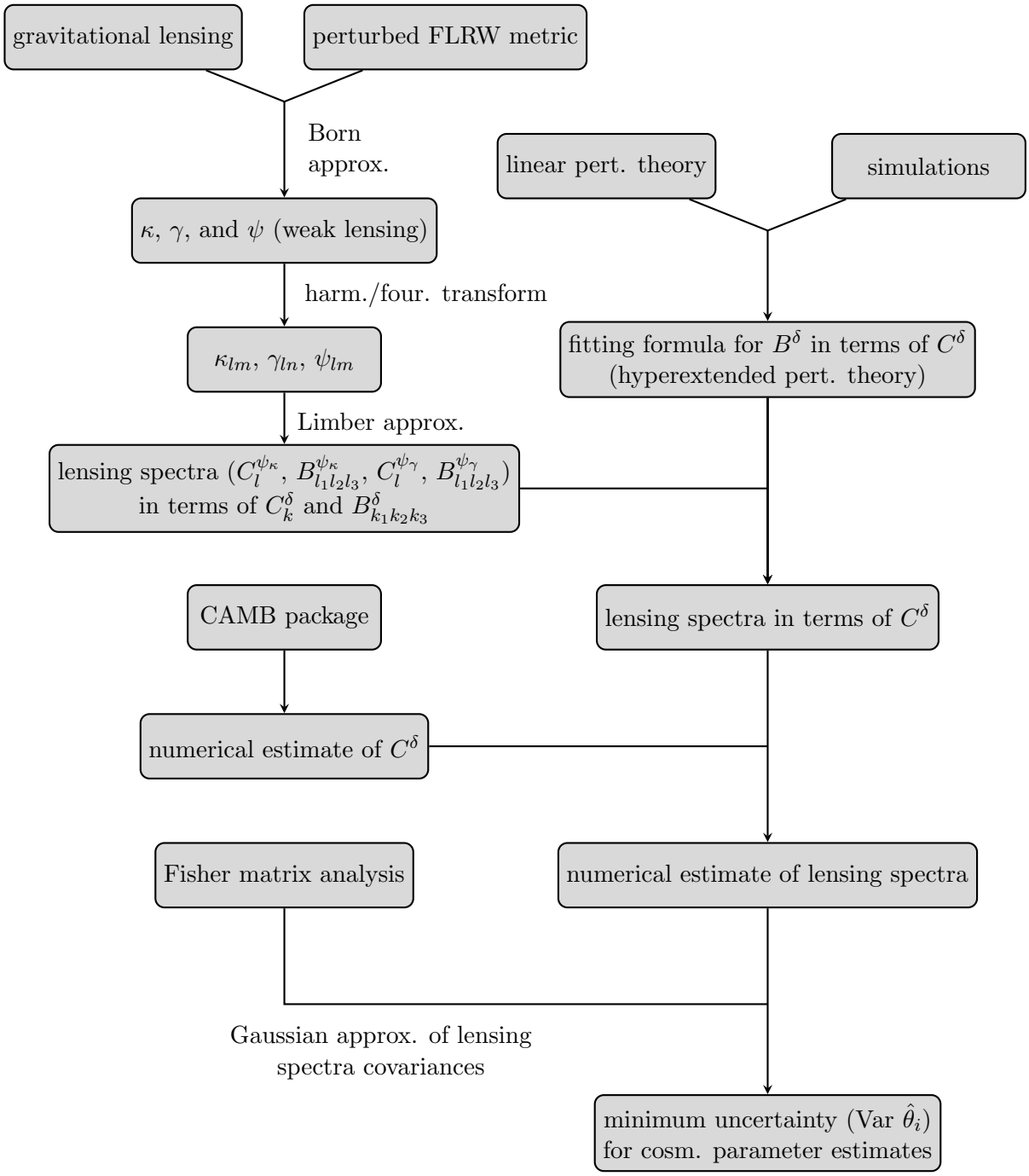

Figure 1: Flowchart of steps involved in calculating the minimum error/uncertainty in cosmological parameter estimates using convergence and shear power- and bi-spectra.

2 Weak Lensing

2.1 Approximations Made / Regime

2.2 Perturbed Photon Paths

Work in **conformal newtonian gauge**. In this section we'll work in units where $c = 1$. Denoting conformal time and conformal radial distance by η and χ, respectively, the perturbed line element is given by

$$\mathrm{d}s^2 = a^2(\eta)((1+2\Psi_N)\mathrm{d}\eta^2 - (1+2\Phi_N)\gamma_{ij}\mathrm{d}x^i\mathrm{d}x^j) \tag{1}$$

where γ_{ij} is the unperturbed line element

$$\gamma_{ij} = \mathrm{d}x^i\mathrm{d}x^j = \mathrm{d}\chi^2 + f_K^2(\chi)(\mathrm{d}\theta^2 + \sin^2\theta\mathrm{d}\phi^2). \tag{2}$$

From here of on work in first order in the scalar potentials Φ_N and Ψ_N. For lensing we consider null-geodesics so $\mathrm{d}s^2 = 0$ and we can rewrite the perturbed line element as

$$\mathrm{d}\hat{s}^2 = (1+4\Psi)\mathrm{d}\eta^2 - \gamma_{ij}\mathrm{d}x^i\mathrm{d}x^j \tag{3}$$

with Ψ the **Weyl Potential** given by $\Psi := (\Psi_N - \Phi_N)/2$. A null geodesic $x^\mu(\hat{\lambda})$ in terms of its affine parameter $(\hat{\lambda})$ satisfies the geodesic equation

$$\frac{\mathrm{d}^2x^\mu}{\mathrm{d}\hat{\lambda}^2} + \Gamma^\mu_{\nu\rho}\frac{\mathrm{d}x^\nu}{\mathrm{d}\hat{\lambda}}\frac{\mathrm{d}x^\rho}{\mathrm{d}\hat{\lambda}} = 0, \tag{4}$$

with $\hat{g}_{\mu\nu}(\mathrm{d}x^\mu/\mathrm{d}\hat{\lambda})(\mathrm{d}x^\nu/\mathrm{d}\hat{\lambda}) = 0$.

In the unperturbed there are incoming radial solutions of the form $\chi = \eta_0 - \eta$. We can express $\hat{\lambda}$ in terms of η using The 0-component of the geodesic equation,

$$\frac{\mathrm{d}^2\eta}{\mathrm{d}\hat{\lambda}^2} + 2(\frac{\mathrm{d}\eta}{\mathrm{d}\hat{\lambda}})^2\frac{\mathrm{d}\Psi}{\mathrm{d}\eta} + 2\frac{\mathrm{d}\eta}{\mathrm{d}\hat{\lambda}}\frac{\mathrm{d}x^i}{\mathrm{d}\hat{\lambda}}\frac{\partial\Psi}{\partial x^i} = 0, \tag{5}$$

where the derivative $\mathrm{d}\Psi/\mathrm{d}\eta = \partial_\eta\Psi + (\mathrm{d}x^i/\mathrm{d}\eta)\partial_i\Psi$ is along the perturbed ray. This allows us to rewrite the other (spatial) geodesic equations as

$$\frac{\mathrm{d}^2x^i}{\mathrm{d}\eta^2} - 2\frac{\mathrm{d}x^i}{\mathrm{d}\eta}(\frac{\mathrm{d}\Psi}{\mathrm{d}\eta} + \frac{\mathrm{d}x^j}{\mathrm{d}\eta}\frac{\partial\Psi}{\partial x^j}) + 2\gamma^{ij}\frac{\partial\Psi}{\partial x^j} + \bar{\Gamma}^i_{jk}\frac{\mathrm{d}x^j}{\mathrm{d}\eta}\frac{\mathrm{d}x^k}{\mathrm{d}\eta} = 0, \tag{6}$$

where $\bar{\Gamma}^i_{jk}$ are the connection coefficients of the unperturbed three geometry γ_{ij}. Without loss of generality we consider an observer located at the origin of the spatial coordinates, meaning we are interested in rays that end at $x^i = 0$. In that case $\mathrm{d}\chi/\mathrm{d}\eta = -1 + O(\Psi)$, $\mathrm{d}\theta/\mathrm{d}\eta = O(\Psi)$ and $\mathrm{d}\phi/\mathrm{d}\eta = O(\Psi)$ (with θ and ϕ angular spatial coordinates). For the case of such rays we can evaluate the connection coefficients and rewrite the spatial geodesic equations as

$$\frac{\partial^2\chi}{\mathrm{d}\eta^2} + 2\frac{\mathrm{d}\Psi}{\mathrm{d}\eta} = 0, \tag{7}$$

$$\frac{\mathrm{d}^2\theta}{\mathrm{d}\eta^2} - 2\frac{\mathrm{d}\ln f_K(\chi)}{\mathrm{d}\chi}\frac{\mathrm{d}\theta}{\mathrm{d}\eta} + \frac{2}{f_K^2(\chi)}\frac{\partial\Psi}{\partial\theta} = 0, \tag{8}$$

$$\frac{\mathrm{d}^2\phi}{\mathrm{d}\eta^2} - 2\frac{\mathrm{d}\ln f_K(\chi)}{\mathrm{d}\chi}\frac{\mathrm{d}\phi}{\mathrm{d}\eta} + \frac{2}{f_K^2(\chi)}\frac{1}{\sin^2(\theta)}\frac{\partial\Psi}{\partial\phi} = 0. \tag{9}$$

Integrating twice and using the null condition we can rewrite the the first equation as

$$\chi = \eta_0 - \eta - 2\int_{\eta_0}^{\eta} \Psi \mathrm{d}\eta', \tag{10}$$

where the integral is along the ray. Since we are working at first order in Ψ we can evaluate the integral along the unperturbed path, this is known as the **Born approximation**.*Next follows a short discussion of why perturbations in observation time can be ignored, include?* Doing the same for the other two equations gives

$$\theta(\eta_0 - \chi_*) = \theta_0 - \int_0^{\chi_*} \mathrm{d}\chi \frac{f_K(\chi_* - \chi)}{f_K(\chi_*) f_K(\chi)} 2\frac{\partial}{\partial\theta}\Psi(\chi\hat{n}, \eta_0 - \chi), \tag{11}$$

$$\phi(\eta_0 - \chi_*) = \theta_0 - \int_0^{\chi_*} \mathrm{d}\chi \frac{f_K(\chi_* - \chi)}{f_K(\chi_*) f_K(\chi)} \frac{2}{\sin^2\theta}\frac{\partial}{\partial\phi}\Psi(\chi\hat{n}, \eta_0 - \chi), \tag{12}$$

where θ_0 and ϕ_0 label the line of sight $\hat{n}$. The displacement vector α indicates the infinitesimal displacement of the lensed rays from their unpetrubed observed angles and is related to θ and ϕ through

$$\alpha_\theta = \theta - \theta_0, \quad \alpha_\phi = \sin^2\theta(\phi - \phi_0).$$

This allows us to summarize the above results as

$$\alpha = -2\int_0^{\chi_*} \mathrm{d}\chi \frac{f_K(\chi_* - \chi)}{f_K(\chi_*) f_K(\chi)} \nabla_{\hat{\mathbf{n}}}\Psi(\chi\hat{\mathbf{n}}; \eta_0 - \chi). \tag{13}$$

When working in the weak field limit (i.e. small spacetime curvature) the 00 component of Einsteins equations give us a poisson equation [11],

$$-\nabla^2\Psi(\mathbf{x}, \eta) = 4\pi G a(\eta)^2 \delta\rho(\mathbf{x}, \eta) \tag{14}$$

where K is 0, 1, or -1 depending on the curvature of the universe, $\Delta = \partial_x^2 + \partial_y^2 + \partial_z^2$ is the 3 dimensional laplace operator, $\delta\bar{\rho}$ is the comoving total energy perturbation (evaluated in the rest-frame of the total energy).

2.3 Convergence, shear

Quantities we are interested in measuring depend on how the lensing vector changes with the observation angle. **Magnification matrix** is defined by

$$A_{ij} := \delta_{ij} + \frac{\partial}{\partial\theta_i}\alpha_i(\hat{\mathbf{n}}). \tag{15}$$

This matrix can then be decomposed in the following form, which immediately gives us definitions for the **convergence**, κ, **shear**, γ_1 and γ_2, and **rotation**, ω:

$$A_i j(\hat{\mathbf{n}}) = \begin{pmatrix} 1 - \kappa - \gamma_1 & -\gamma_2 + \omega \\ -\gamma_2 - \omega & 1 - \kappa + \gamma_1 \end{pmatrix}. \tag{16}$$

At 1st order A is a symetric matrix by definition and so ω has to be 0, we will ignore it from here on out. Intuitively, A tells you how a small patch in the sky transforms due to weak lensing, i.e. if you have surface brightness I then

$$I_{\text{emitted}}(\hat{\mathbf{n}} + \delta) = I_{\text{observed}}((\hat{\mathbf{n}} + \delta) + \alpha(\hat{\mathbf{n}} + \delta)) \approx I_{\text{observed}}((\hat{\mathbf{n}} + \alpha + A_{ij}\delta_j). \tag{17}$$

given that $|A_{ij}| = (1 - \kappa)^2 + \omega^2 - |\gamma|^2 = 1 - 2\kappa + O(\kappa^2, \gamma^2, \omega^2)$, we can interpret κ as telling us about the overal magnification of the source. The γ_i represent the area preserving distortion, i.e. stretching and squeezing in a specific direction.

2.4 lensing potential

Taking the derivative out of the integral in equation REF leads us to defining the **lensing potential**, ψ,

$$\alpha = \nabla_{\hat{\mathbf{n}}}\psi, \quad \psi(\hat{\mathbf{n}}) = -2\int_0^{\chi_*} \mathrm{d}\chi \frac{f_K(\chi_* - \chi)}{f_K(\chi_*)f_K(\chi)}\Psi(\chi\hat{\mathbf{n}}; \eta_0 - \chi). \tag{18}$$

We can relate κ and γ directly to the lensing potential as

$$\kappa = \frac{1}{2}\nabla^2\psi, \quad \gamma_1 = \frac{1}{2}(\partial_\theta^2 - \partial_\phi^2)\psi, \quad \gamma_2 = \partial_\theta\partial_\phi\psi. \tag{19}$$

2.5 Regarding window functions

The window function for light emitted from a source at fixed radius χ_* is $(\chi - \chi^*)/(\chi_*\chi)$, if the source is instead distributed over the radius as $p(\chi)$, with $p(\chi)$ normalized to integrate to 1, we generalize the window function as

$$W(\chi) = \int_\chi^{\chi_*} \mathrm{d}\chi' p(\chi')\frac{\chi' - \chi}{\chi'\chi}.$$

The integration limit is up to surface of last scattering because further than that no source can contribute to the observed image. In the case of an image of the CMB we can take $p(\chi') = \delta(\chi' - \chi_*)$, in which case the window function reduces back to $(\chi_* - \chi)/(\chi_*\chi)$. In the case of different sources, we will differentiate between their respective window functions with a subscript. In this case the factor that changes is the distribution function. The sources considered in this paper are only the CMB and selections of galaxies from galaxy surveys.

3 Weak Lensing Statistics

3.1 Lensing Potential Powerspectrum

Consider the lensing potential, ψ, then decomposing into spherical harmonics gives

$$\psi(\hat{\mathbf{n}}) = \sum_{lm} \psi_{lm} Y_{lm}(\hat{\mathbf{n}}). \tag{20}$$

On the other hand, consider the decomposition of Ψ in fourier modes with the Fourier convention $\Psi(\mathbf{x}, \eta) = \int \frac{\mathrm{d}^3\mathbf{k}}{(2\pi)^3}\Psi(\mathbf{k}, \eta)e^{i\mathbf{k}\cdot\mathbf{x}}$,

$$\psi(\hat{\mathbf{n}}) = -2\int_0^{\chi_*} \mathrm{d}\chi W(\chi)\int \frac{\mathrm{d}^3\mathbf{k}}{(2\pi)^3}\Psi(\mathbf{k}, \eta_0 - \chi)e^{i\mathbf{k}\cdot\hat{\mathbf{n}}\chi}. \tag{21}$$

We can than relate the multipole modes of ψ to the fourier modes of Ψ through

$$\psi_{lm} = \langle Y_l^m|\psi\rangle = \int \mathrm{d}^2\hat{\mathbf{n}} Y_l^m(\hat{\mathbf{n}})^*\psi(\hat{\mathbf{n}}) \tag{22}$$

$$= -2\int \mathrm{d}^2\hat{\mathbf{n}} Y_l^m(\hat{\mathbf{n}})^* \int_0^{\chi_*} \mathrm{d}\chi W(\chi)\int \frac{\mathrm{d}^3\mathbf{k}}{(2\pi)^3}\Psi(\mathbf{k}, \eta_0 - \chi)e^{i\mathbf{k}\cdot\hat{\mathbf{n}}\chi} \tag{23}$$

Now define the power spectrum as

$$\langle \Psi(\mathbf{k},\eta)\Psi^*(\mathbf{k}',\eta')\rangle = \frac{2\pi^2}{k^3}P_\Psi(k,\eta,\eta')\delta(\mathbf{k}-\mathbf{k}'), \tag{24}$$

with η denoting the conformal time. This gives

$$\langle \psi(\hat{\mathbf{n}})\psi(\hat{\mathbf{n}}')\rangle = 4\int_0^{\chi_*} \mathrm{d}\chi \int_0^{\chi_*} \mathrm{d}\chi' W(\chi)W(\chi') \int \frac{\mathrm{d}^3\mathbf{k}}{(2\pi)^6}\frac{2\pi^2}{k^3}P_\psi(k,\eta_0-\chi,\eta_0-\chi')e^{i\mathbf{k}\cdot\hat{\mathbf{n}}\chi}e^{i\mathbf{k}\cdot\hat{\mathbf{n}}'\chi'}, \tag{25}$$

where we used that $\eta = \eta_0 - \chi$ along the unperturbed photon path (Born approximation), with η_0 the time at which the light ray hits earth. We can use the result

$$e^{i\mathbf{k}\cdot\hat{\mathbf{n}}\chi} = 4\pi\sum_{lm} i^l j_l(k\chi)Y_l^m(\hat{\mathbf{n}})^*Y_l^m(\hat{\mathbf{k}}) = 4\pi\sum_{lm} i^l j_l(k\chi)Y_l^m(\hat{\mathbf{n}})Y_l^m(\hat{\mathbf{k}})^*, \tag{26}$$

where j_l is the spherical Bessel function (ELABORATE ON THIS?), to rewrite the above equation. Using both versions of the identity above, we immedatialy get a factor $Y_l^m(\hat{\mathbf{k}})Y_{l'}^{m'}(\hat{\mathbf{k}})^*$ in our integral. We can factor the differential element of $\mathrm{d}^3\mathbf{k}$ into a radial and angular part as $k^2\mathrm{d}k\mathrm{d}^2\Omega_k$, with Ω_k the solid angle, to apply the orthonormality condition of the spherical harmonics. Note that we take the same sequence of steps a number of times in other parts of the derivations of the lensing spectra. We thus obtain

$$\langle \psi(\hat{\mathbf{n}})\psi(\hat{\mathbf{n}}')\rangle = 4(4\pi)^2\sum_{ll'mm'} i^{l+l'}\int_0^{\chi_*}\mathrm{d}\chi\int_0^{\chi_*}\mathrm{d}\chi' W(\chi)W(\chi') \tag{27}$$

$$\times\int\frac{k^2\mathrm{d}k}{(2\pi)^6}\frac{2\pi^2}{k^3}j_l(k\chi)j_{l'}(k\chi')P_\psi(k,\eta_0-\chi,\eta_0-\chi')Y_{lm}(\hat{\mathbf{n}})Y_{l'm'}(\hat{\mathbf{n}}')^*\delta_{ll'}\delta_{mm'}. \tag{28}$$

The angular power spectrum is defined similarly to the power spectrum, i.e.

$$\langle \psi_{lm}\psi^*_{l'm'}\rangle = \delta_{ll'}\delta_{mm'}C_l^\psi. \tag{29}$$

Note that the correlation is independent of m and m'. We can thus read from equation 28 that

$$C_l^\psi = 4(4\pi)^2(-1)^l\int_0^{\chi_*}\mathrm{d}\chi\int_0^{\chi_*}\mathrm{d}\chi' W(\chi)W(\chi')\int\frac{k^2\mathrm{d}k}{(2\pi)^6}\frac{2\pi^2}{k^3}j_l(k\chi)j_l(k\chi')P_\psi(k,\eta_0-\chi,\eta_0-\chi'), \tag{30}$$

which can be simplified to

$$C_l^\psi = (-1)^l\frac{2}{\pi^2}\int_0^{\chi_*}\mathrm{d}\chi\int_0^{\chi_*}\mathrm{d}\chi' W(\chi)W(\chi')\int k^2\mathrm{d}k j_l(k\chi)j_l(k\chi')\frac{P_\psi(k,\eta_0-\chi,\eta_0-\chi')}{k^3}. \tag{31}$$

To further evaluate the integral we will make the standard **Limber approximation**. The Bessel functions peak sharply at $l = x$[1], with the peak being increasingly sharp for higher l. Similarly to $\delta(x-x_0)f(x) = \delta(x-x_0)f(x_0)$, we thus take $j_l(k\chi)f(k) \approx j_l(k\chi)f(l/\chi)$. The Bessel functions satisfy an orthogonality condtion,

$$\int k^2\mathrm{d}k j_l(k\chi)j_l(k\chi') = \frac{\pi}{2\chi^2}\delta(\chi-\chi'). \tag{32}$$

[1]Some sources use $x \approx l + 1/2$ instead, which is slightly more accurate for larger scales (low l) and slightly less accurate for smaller scales.

In combination with the Limber approximation we thus find

$$\int k^2 \mathrm{d}k j_l(k\chi) j_l(k\chi') f(k) \approx \frac{\pi}{2\chi^2}\delta(\chi-\chi') f(l/\chi). \tag{33}$$

It allows us to write the Limber-approximate angular spectrum as

$$C^\psi(l) = (-1)^l \frac{2}{\pi^2}\int_0^{\chi_*} \mathrm{d}\chi \int_0^{\chi_*} \mathrm{d}\chi' W(\chi)W(\chi')\frac{\pi}{2\chi^2}\delta(\chi-\chi')\frac{\chi^3}{l^3}P_\psi(l/\chi, \eta_0-\chi, \eta_0-\chi') \tag{34}$$

$$= (-1)^l \frac{1}{l^3\pi}\int_0^{\chi_*} \chi \mathrm{d}\chi W(\chi)^2 P_\psi(l/\chi, \eta_0-\chi, \eta_0-\chi). \tag{35}$$

3.2 Lensing potential bispectrum

The derivation of the bispectrum proceeds similarly to that of the power spectrum. We aim to compute the bispectrum of the lensing potential fields of 3 (possibly distinct sources), ψ_1, ψ_2, ψ_3.

$$\langle (\psi_1)_{l_1m_1}(\psi_2)_{l_2m_2}(\psi_3)_{l_3m_3}\rangle = \prod_i \left(-2\int \mathrm{d}^2\hat{\mathbf{n}}_i (Y_{l_i}^{m_i}(\hat{\mathbf{n}}_i))^* \int_0^{\chi_*} \mathrm{d}\chi_i W_i(\chi_i) \int \frac{\mathrm{d}^3\mathbf{k}_i}{(2\pi)^3} e^{i\mathbf{k}_i\cdot\hat{\mathbf{n}}_i\chi_i}\right)$$
$$\times \langle \prod_i \Psi(\mathbf{k}_i, \eta_0-\chi_i)\rangle.$$

Defining the bispectrum of the graviational potential as

$$\langle \prod_{i=1,2,3} \Psi(\mathbf{k}_i, \eta_0-\chi_i)\rangle = (2\pi)^3\delta(\mathbf{k}_1+\mathbf{k}_2+\mathbf{k}_3)B^\Psi(\{k_i\},\{\eta_0-\chi_i\}),$$

we rewrite the lensing potential bispecrum as

$$\langle (\psi_1)_{l_1m_1}(\psi_2)_{l_2m_2}(\psi_3)_{l_3m_3}\rangle = \prod_i \left(-2\int \mathrm{d}^2\hat{\mathbf{n}}_i (Y_{l_i}^{m_i}(\hat{\mathbf{n}}_i))^* \int_0^{\chi_*} \mathrm{d}\chi_i W_i(\chi_i) \int \frac{\mathrm{d}^3\mathbf{k}_i}{(2\pi)^3} e^{i\mathbf{k}_i\cdot\hat{\mathbf{n}}_i\chi_i}\right)$$
$$\times (2\pi)^3\delta(\mathbf{k}_1+\mathbf{k}_2+\mathbf{k}_3)B^\Psi(\{k_i\},\{\eta_0-\chi_i\}).$$

Now using the identity REF for the complex exponential:

$$\langle (\psi_1)_{l_1m_1}(\psi_2)_{l_2m_2}(\psi_3)_{l_3m_3}\rangle$$
$$= \prod_i \left(-2\int \mathrm{d}^2\hat{\mathbf{n}}_i (Y_{l_i}^{m_i}(\hat{\mathbf{n}}_i))^* \int_0^{\chi_*} \mathrm{d}\chi_i W_i(\chi_i) \int \frac{\mathrm{d}^3\mathbf{k}_i}{(2\pi)^3} 4\pi \sum_{lm} i^l j_l(k_i\chi_i) Y_l^m(\hat{\mathbf{n}}_i) Y_l^m(\hat{\mathbf{k}}_i)^*\right)$$
$$\times (2\pi)^3\delta(\mathbf{k}_1+\mathbf{k}_2+\mathbf{k}_3)B^\Psi(\{k_i\},\{\eta_0-\chi_i\})$$
$$= \left[\prod_i \left(-2\int_0^{\chi_*} \mathrm{d}\chi_i W_i(\chi_i) \int \frac{\mathrm{d}^3\mathbf{k}_i}{(2\pi)^3} 4\pi i^{l_i} j_{l_i}(k_i\chi_i) Y_{l_i}^{m_i}(\hat{\mathbf{k}}_i)^*\right)\right](2\pi)^3\delta(\mathbf{k}_1+\mathbf{k}_2+\mathbf{k}_3)B^\Psi(\{k_i\},\{\eta_0-\chi_i\}).$$

We can write the 3D dirac delta function in terms of spherical harmonics as

$$\delta(\mathbf{k}_1+\mathbf{k}_2+\mathbf{k}_3) = 8\int \mathrm{d}^3\mathbf{x} \prod_{i=1,2,3}\left(\sum_{l_jm_j} i^{l_j} j_{l_j}(k_i x) Y_{l_j}^{m_j}(\hat{\mathbf{k}}_i) Y_{l_j}^{m_j}(\hat{\mathbf{x}})^*\right).$$

This results in

$$\langle(\psi_1)_{l_1m_1}(\psi_2)_{l_2m_2}(\psi_3)_{l_3m_3}\rangle = \prod_i \left(-2\int_0^{\chi_*} \mathrm{d}\chi_i W_i(\chi_i) \int \frac{\mathrm{d}^3\mathbf{k}_i}{(2\pi)^3} 4\pi i^{l_i} j_{l_i}(k_i\chi_i) Y_{l_i}^{m_i}(\hat{\mathbf{k}_i})^*\right)$$
$$\times(2\pi)^3 8 \int \mathrm{d}^3\mathbf{x} \prod_i \left(\sum_{lm} i^l j_l(k_i x) Y_l^m(\hat{\mathbf{k}_i}) Y_l^m(\hat{\mathbf{x}})^*\right) B^\Psi(\{k_i\},\{\eta_0-\chi_i\})$$
$$= (2\pi)^3 8 \int \mathrm{d}^3\mathbf{x} \prod_i \left(-2\int_0^{\chi_*} \mathrm{d}\chi_i W_i(\chi_i) \int \frac{k_i^2 \mathrm{d}k_i}{(2\pi)^3} 4\pi(-1)^{l_i} j_{l_i}(k_i\chi_i) j_{l_i}(k_i x) Y_{l_i}^{m_i}(\hat{\mathbf{x}})^*\right) B^\Psi(\{k_i\},\{\eta_0-\chi_i\})$$

The angular part of the $\mathbf{x}$ integral can be evaluated using the identity

$$\int \mathrm{d}\Omega_{\hat{n}}\, Y^*_{l_1m_1}(\hat{x}) Y^*_{l_2m_2}(\hat{n}) Y^*_{l_3m_3}(\hat{n}) = (-1)^{m_1+m_2+m_3} \int \mathrm{d}\Omega_{\hat{n}}\, Y_{l_1-m_1}(\hat{n}) Y_{l_2-m_2}(\hat{n}) Y_{l_3-m_3}(\hat{n})$$
$$= (-1)^{m_1+m_2+m_3} \sqrt{\frac{(2l_1+1)(2l_2+1)(2l_3+1)}{4\pi}} \begin{pmatrix} l_1 & l_2 & l_3 \\ 0 & 0 & 0 \end{pmatrix} \begin{pmatrix} l_1 & l_2 & l_3 \\ -m_1 & -m_2 & -m_3 \end{pmatrix} \equiv A_{\mathrm{l}}^{\mathbf{m}},$$

giving

$$\langle(\psi_1)_{l_1m_1}(\psi_2)_{l_2m_2}(\psi_3)_{l_3m_3}\rangle = (2\pi)^3 8 A_{\mathrm{l}}^{\mathbf{m}} \int x^2 \mathrm{d}x \prod_i \left(-2\int_0^{\chi_*} \mathrm{d}\chi_i W_i(\chi_i) \int \frac{k_i^2 \mathrm{d}k_i}{(2\pi)^3} 4\pi(-1)^{l_i} j_{l_i}(k_i\chi_i) j_{l_i}(k_i x)\right)$$
$$\times B^\Psi(\{k_i\},\{\eta_0-\chi_i\}).$$

Now applying the Limber approximation again:

$$\langle(\psi_1)_{l_1m_1}(\psi_2)_{l_2m_2}(\psi_3)_{l_3m_3}\rangle = (2\pi)^3 8 A_{\mathrm{l}}^{\mathbf{m}} \int x^2 \mathrm{d}x \prod_i \left(-2\int_0^{\chi_*} \mathrm{d}\chi_i W_i(\chi_i) \frac{1}{(2\pi)^3} \frac{\pi}{2\chi_i^2} \delta(x-\chi_i) 4\pi(-1)^{l_i}\right)$$
$$\times B^\Psi(\{l_i/\chi_i\},\{\eta_0-\chi_i\})$$
$$= (2\pi)^3 8 A_{\mathrm{l}}^{\mathbf{m}} \int \chi^2 \mathrm{d}\chi \prod_i \left(-2W_i(\chi) \frac{1}{(2\pi)^3} \frac{\pi}{2\chi^2} 4\pi(-1)^{l_i}\right) B^\Psi(\{l_i/\chi\},\eta_0-\chi).$$

Finally, we aim to rewrite the above in terms of the angular bispectrum of the lensing potential.

The definition for the bispectrum of any set of randomly distributed spherical harmonic components X^k_{lm} is CITE Hu 2000

$$\langle(X_1)_{l_1m_1}(X_2)_{l_2m_2}(X_3)_{x_3m_3}\rangle = \begin{pmatrix} l_1 & l_2 & l_3 \\ m_1 & m_2 & m_3 \end{pmatrix} B^{X_1X_2X_3}_{l_1l_2l_3}.$$

Note the independence on m_i, this necesarilly follows from statistical isotropy. If $m_1+m_2+m_3 \neq 0$, the associated Wigner-3j symbol vanishes and the bispectrum is set to zero. Also note that in this definition we have immediately generalized to include cross correlation between different fields X_1, X_2, X_3. This will be relevant later when we look at cross correlations between shear and convergence fields.

Using the above definition and the symmetry property

$$\begin{pmatrix} l_1 & l_2 & l_3 \\ -m_1 & -m_2 & -m_3 \end{pmatrix} = (-1)^{l_1+l_2+l_3} \begin{pmatrix} l_1 & l_2 & l_3 \\ m_1 & m_2 & m_3 \end{pmatrix}$$

we find

$$B^{\psi_1\psi_2\psi_3}_{l_1l_2l_3} = (-1)^{l_1+l_2+l_3}\sqrt{\frac{(2l_1+1)(2l_2+1)(2l_3+1)}{4\pi}}\begin{pmatrix} l_1 & l_2 & l_3 \\ 0 & 0 & 0\end{pmatrix}(2\pi)^3 8$$
$$\times\int \chi^2 \mathrm{d}\chi \prod_i \left(-2W_i(\chi,\chi_*)\frac{1}{(2\pi)^3}\frac{\pi}{2\chi^2}4\pi(-1)^{l_i}\right) B^\Psi(\{l_i/\chi\},\{\eta_0-\chi\}),$$

where we were able to drop the $(-1)^{m_1+m_2+m_3}$ factor due to the bispecrum vanishing if that sum doesn't equal 0, as mentioned earlier. When all m_i equal zero, the Wigner 3j-symbol gains a number of useful properties In particular, it vanishes if $l_1+l_2+l_3$ is odd, meaning we can drop the $(-1)^{l_1+l_2+l_3}$ factor. Additionally cancelling common factors then gives

$$B^{\psi_1\psi_2\psi_3}_{l_1l_2l_3} = -\sqrt{\frac{(2l_1+1)(2l_2+1)(2l_3+1)}{4\pi}}\begin{pmatrix} l_1 & l_2 & l_3 \\ 0 & 0 & 0\end{pmatrix} 8\int \frac{\mathrm{d}\chi}{\chi^4} W_1(\chi)W_2(\chi)W_3(\chi)B^\Psi(\{l_i/\chi\},\eta_0-\chi).$$

3.3 Gravitational potential spectra in terms of matter spectra

To convert equations ... and ... to forms that we can directly evaluate we will need to replace the spectra of the graviational potential with matter spectra. Specifically, we define the matter power spectrum in agreement with the CAMB package documentation CITE and the matter bispectrum in agreement with CITE FITTING FUNC PAPER such that we can approximate it in terms of the matter power spectrum using hyperextended perturbation theory. The **density contrast** is defined as

$$\delta(\mathbf{x}) := \frac{\rho(\mathbf{x})-\bar{\rho}}{\bar{\rho}}, \tag{36}$$

and the matter spectra are defined in terms of the fourier transformed density contrast $\delta(\mathbf{k})$ as

$$\langle\delta(\mathbf{k},\eta)\delta(\mathbf{k}',\eta)^*\rangle = (2\pi)^3\delta(\mathbf{k}-\mathbf{k}')P^\delta(\mathbf{k},\eta),$$
$$\langle\delta(\mathbf{k}_1,\eta)\delta(\mathbf{k}_2,\eta)\delta(\mathbf{k}_3,\eta)\rangle = (2\pi)^3\delta(\mathbf{k}_1+\mathbf{k}_2+\mathbf{k}_3)B^\delta(k_1,k_2,k_3,\eta).$$

The mean matter density of the universe, $\bar{\rho}$, can be expressed in terms of the matter density parameter Ω_m and the critical density ρ_c as

$$\bar{\rho}(\eta) = \frac{3\Omega_m H_0^2}{8\pi G}\frac{1}{a(\eta)^3},$$

where $a(\eta)$ is the only time dependent factor on the right hand side. In the case of a flat universe ($K=0$) we can thus rewrite the Poisson equation REF (6.41 in modern cosmology) as

$$-\nabla^2\Psi = 4\pi G a^2\left(\frac{3\Omega_m H_0^2}{8\pi G}\frac{1}{a^3}\right)\delta = \frac{3\Omega_m H_0^2}{2}\frac{1}{a}\delta \implies \Psi(k,\eta) = \frac{3\Omega_m H_0^2}{2}\frac{1}{a}\frac{\delta(k,\eta)}{k^2}, \tag{37}$$

where $\Psi(k,\eta)$ and $\delta(k,\eta)$ are functions in Fourier space. For the power- and bispectra we find

$$\langle\Psi(\mathbf{k},\eta)\Psi^*(\mathbf{k}',\eta)\rangle = \frac{2\pi^2}{k^3}P^\Psi(k,\eta)\delta(\mathbf{k}-\mathbf{k}') \implies P^\Psi(k,\eta) = \frac{1}{k}(9\Omega_m^2 H_0^4\pi)\frac{1}{a^2}P^\delta(k,\eta),$$
$$\langle\Psi(\mathbf{k}_1,\eta)\Psi(\mathbf{k}_2,\eta)\Psi(\mathbf{k}_3,\eta)\rangle = (2\pi)^3\delta(\mathbf{k}_1+\mathbf{k}_2+\mathbf{k}_3)B^\Psi(k_1,k_2,k_3,\eta)$$
$$\implies B^\Psi(k_1,k_2,k_3,\eta) = \frac{1}{k_1^2k_2^2k_3^2}\left(\frac{3\Omega_m H_0^2}{2}\right)^3\frac{1}{a^3}B^\delta(\{k_i\},\eta).$$

We conclude this section by using the above equations to rewrite the lensing potential spectra (equations REF and REF) in terms of matter spectra

$$\boxed{\begin{aligned} P_l^{\psi_X\psi_Y} &= (-1)^l \frac{9}{l^4}\Omega_m^2 H_0^4 \int_0^{\chi_*} \chi^2 \mathrm{d}\chi a(\eta_0-\chi)^{-2} W_X(\chi) W_Y(\chi) P^\delta(l/\chi, \eta_0-\chi), \\ B_{l_1 l_2 l_3}^{\psi_X\psi_Y\psi_Z} &= -\sqrt{\frac{(2l_1+1)(2l_2+1)(2l_3+1)}{4\pi}} \begin{pmatrix} l_1 & l_2 & l_3 \\ 0 & 0 & 0 \end{pmatrix} \frac{27}{l_1^2 l_2^2 l_3^2}\Omega_m^3 H_0^6 \\ &\quad \times \int \chi^2 \mathrm{d}\chi a(\eta_0-\chi)^{-3} W_X(\chi) W_Y(\chi) W_Z(\chi) B^\delta(\{l_i/\chi\}, \eta_0-\chi). \end{aligned}}$$

3.4 Convergence and shear multipole moments

Convergence Taking the harmonic decomposition of the convergence,

$$\kappa(\hat{\mathbf{n}}) = \kappa_{lm} Y_l^m(\hat{\mathbf{n}}), \tag{38}$$

you can relate it to the multipole moments of the lensing potential through CHECK FACTOR OF 2

$$\kappa_{lm} = \frac{1}{2}(\nabla^2\psi)_{lm} = \frac{l(l+1)}{2}\psi_{lm} \tag{39}$$

because the spherical harmonics are eigenfunctions of the Laplacian operator.

Shear On the other hand, the shear is given by

$$\gamma = \gamma_1 + i\gamma_2 = \frac{1}{2}\eth_1(\eth_0\psi) \tag{40}$$

where the spin raising operator, $\eth_s$ acts on a spin s function defined on S^2 to create a spin $s+1$ function. The above equality is proven explicitely in appendix ... $\eth_s$ can be written in (θ,ϕ) coordinates as

$$\eth_s = -\sin^s\theta(\partial_\theta + \frac{i}{\sin\theta})\frac{1}{\sin^s\theta}. \tag{41}$$

It is worth explaining that in this context a spin s function referes to a function ${}_sf(\theta,\phi)$ that transforms under any rotation of coordinates by picking up a phase factor $e^{is\alpha}$, with α the angle of the rotation, i.e.

$$f'(\theta',\phi') = e^{is\alpha} f(\theta,\phi). \tag{42}$$

Shear is actually a spin 2 function, which can immediately be seen by observing that rotating a galaxy image stretched and squeezed through weak lensing by 180 degrees gives the same stretching and squeezing, i.e. the same shear. It is thus expected that the shear is proportional to $\eth^2\psi$.

The spin weighted spherical harmonics, ${}_sY_l^m$ are eigenfunctions of the raising/lowering operator, in particular

$$\eth_s Y_l^m = \sqrt{(l-s)(l+s+1)}_{s+1} Y_l^m. \tag{43}$$

Decomposing the shear as

$$\gamma(\theta,\phi) = \gamma_{lms} Y_l^m(\theta,\phi), \tag{44}$$

we thus find

$$\gamma_{lm} = \frac{1}{2}\sqrt{(l-1)(l)(l+1)(l+2)}\psi_{lm} \tag{45}$$

4 Calculation Details

4.1 Numerical Considerations

Running cosmological simulations to obtain the matter power spectra and other functions was done with the CAMB package (REF).

The derivatives of the lensing spectra were done numerically using a four point central difference formula, given by

$$f'(x) = \frac{-f(x+2h) + 8f(x+h) - 8f(x-h) + f(x-2h)}{12h} + \mathcal{O}(h^4).$$

h was chosen to be 2.5% of the x value. Testing showed this to generally be the best choise to avoid both the inacuracies from numerical errors (relevant for small h) and inacuracies due to the $\mathcal{O}(h^4)$ error inherent in the four point finite difference formula. The derivative w.r.t. σ_8 was an exception as it could not be taken by varying it directly and so was calculated implicitly using the chain rule.

To speed up the calculation of the lensing powerspectra and especially the bispectra, an interpolation approach was used. Due to being 3 dimensional, it was not feasible to interpolate the lensing bispectrum directly. We instead chose to interpolate all 1 and 2 dimensional functions that the bispectra are based on and then calculate the bispectra with the interpolated functions instead. This significantly sped up the computation at the cost of small errors in the values in the bispectrum ($\sim 1\%$) when compared with the uninterpolated values.

The time complexity of the Fisher matrix scales with the maximum multipole considered, l_{max}, as $\mathcal{O}(l_{max}^3)$, leading to time issues for realistic values of l_{max}. We thus calculated the $l_1 < l_2 < l_3$ part of each Fisher matrix element (see appendix (REF)) by sampling every step of 10 (CHECK IF THIS IS STILL CORRECT BEFORE PUBLISHING) in l_1 and l_2. Due to the discontinuos nature of the bispectrum (e.g. it vanishes immediately if $l_1 + l_2 + l_3$ is and odd number) we didn't sample l_3 values. This was done similarly in (REF).

The matter bispectrum was calculated from the matter powerspectrum using a fitting formula based on perturbation theory [12]. The bispectrum is given by

$$B_m(k_1, k_2, k_3, \chi) = 2F_2(k_1, k_2, z)P_m(k_1, z)P_m(k_2, z) + 2 \text{ perm.} \tag{46}$$

where P_m is the matter power spectrum, and the kernel F_2 is given by:

$$F_2(k_1, k_2, z) = \frac{5}{7}a(k_1, z)a(k_2, z) + \frac{k_1^2 + k_2^2}{2k_1k_2}b(k_1, z)b(k_2, z)\cos\theta + \frac{2}{7}c(k_1, z)c(k_2, z)\cos^2\theta. \tag{47}$$

The functions $a(k, z)$, $b(k, z)$, and $c(k, z)$ are defined as:

$$a(k, z) = \frac{1 + \sigma_8^{a_6}(z)\sqrt{0.7}Q(n_{\text{eff}})(q^{a_1})^{n_{\text{eff}}+a_2}}{1 + (q^{a_1})^{n_{\text{eff}}+a_2}}, \tag{48}$$

$$b(k, z) = \frac{1 + 0.2a_3(n_{\text{eff}} + 3)(q^{a_7})^{n_{\text{eff}}+3+a_8}}{1 + (q^{a_5})^{n_{\text{eff}}+3.5+a_8}}, \tag{49}$$

$$c(k,z) = \frac{1 + \left[\frac{4.5a_4}{1.5+(n_{\rm eff}+3)^4}\right](q^{a_5})^{n_{\rm eff}+3+a_9}}{1 + (q^{a_5})^{n_{\rm eff}+3.5+a_9}}. \tag{50}$$

Here, $Q(n_{\rm eff})$ is given by:

$$Q(x) = \frac{4-2x}{1+2^{x+1}}. \tag{51}$$

The effective spectral index of the linear power spectrum is defined as:

$$n_{\rm eff} \equiv \frac{d\ln P_m^{\rm lin}(k)}{d\ln k}. \tag{52}$$

Additionally, q is given by:

$$q = \frac{k}{k_{\rm NL}}, \tag{53}$$

where $k_{\rm NL}$ is the scale at which nonlinearities become significant, satisfying:

$$4\pi k_{\rm NL}^3 P_m^{\rm lin}(k_{\rm NL}) = 1. \tag{54}$$

The coefficients a_i are:

$$\begin{aligned} &a_1 = 0.484, \quad a_2 = 3.740, \quad a_3 = -0.849, \quad a_4 = 0.392, \\ &a_5 = 1.013, \quad a_6 = -0.575, \quad a_7 = 0.128, \quad a_8 = -0.722, \quad a_9 = -0.926. \end{aligned}$$

4.2 Choosing Experimental Parameters

We chose our fiducial cosmology in line with the results from the Planck mission [2].

$$\begin{aligned} H_0 &= 67.4\,\text{km/s/Mpc}, && \text{(Hubble constant)} \\ \Omega_b h^2 &= 0.0224, && \text{(Physical baryon density parameter)} \\ \Omega_c h^2 &= 0.120, && \text{(Physical cold dark matter density parameter)} \\ n_s &= 0.965, && \text{(Scalar spectral index)} \\ A_s &= 2.1 \times 10^{-9}, && \text{(Amplitude of primordial scalar fluctuations)} \\ \sum m_\nu &= 0.06\,\text{eV}, && \text{(Sum of neutrino masses)} \\ w_0 &= -1. && \text{(Dark energy equation of state parameter)} \end{aligned}$$

For the parameter constraints we took the multipole range to be from 50 (l_{min}) to 1000 (l_{max}) (INCREASE TO 2000?) (CHECK BEFORE PUBLISHING) in line with measurement ranges from current gen surveys (PROOF BY LOOKING AT ACTUALL EXPERIMENTS).

We will consider multiple possibilities for the other calculation parameters (noise levels and redshift distribution of observed galaxies). This is done to allow us to more accurately model constraints from measurements by the Simons Observatory (SO), CMB-S4, Euclid, and Large Synoptic Survey Telescope (LSST) surveys. The first two measure CMB lensing while the latter two measure lensing shear of galaxies.

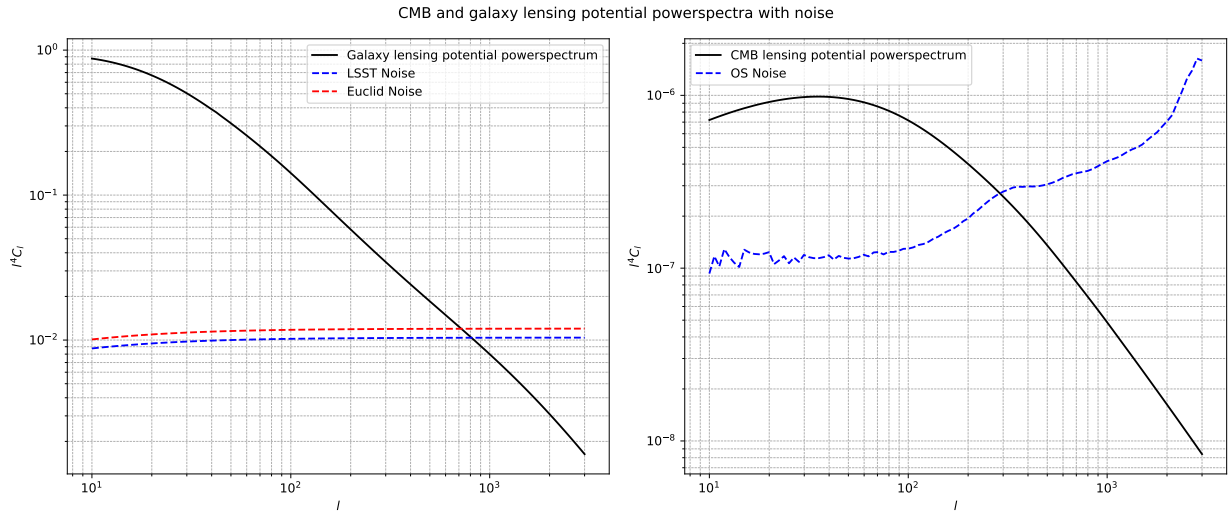

Figure 2: CMB and galaxy lensing potential power spectra with noise. The left panel shows the galaxy lensing potential power spectrum with LSST and Euclid noise, while the right panel shows the CMB lensing potential power spectrum with OS noise.

The noise levels in the CMB lensing are caused by a variety of factors, see e.g. [22]. The noise curves for the SO are shown alongside a simulated pure convergence power spectrum curve in figure 2. This is the noise source we use for CMB lensing.

For shear measurements, the noise is simpler to model as the primary source is shot noise due to the discrete number of galaxies in each patch of the survey. The mean ellipiticity of the galaxies in a patch is calculated and a deviation from the mean is interpreted as lensing shear. The greater the number of galaxies the more accurately can the mean ellipticity be determined. Choosing the size of the patch is a balancing between signal to noise and resolution. Smaller patches give more uncertain shear measurements while providing better overal resolution for the shear map and thus allowing measurements of shear bi- and powerspectra to higher multipole numbers. The opposite is true for larger patch sizes. The power spectrum of the shear noise is given by

$$N_l^{\gamma\gamma} = \frac{\sigma_{rms}^2}{\bar{n}_g}$$

where $\bar{n}_g$ is the mean number of galaxies observed per sterradian accross the whole survey [24]. and σ_γ^2 is the intrinsic ellipticity dispersion. Euclid and the LSST both have $\sigma_{rms} \approx 0.26$ [23] [9]. Euclid is expected to measure a galaxy density of approximately 30 galaxies per square arcminute [26] while LSST aims to measure 26 [8] The noise levels are graphed alongside a simulated shear power spectrum in figure 2. We perform our calculations with Euclid noise levels throughout this paper. The redshift distribution of the observed galaxies is commonly parameterized as [4]

$$n(z) \propto z^a \exp\left[-\left(\frac{z}{z_0}\right)^b\right].$$

We choose the parameter combination $a = 2$, $b = 3/2$ and $z_0 = 0.64$ which is similar to the expected distributions of Euclid, (which will probe primarily in the 0.2 - 2.6 redshift range [10]) and the LSST mission (which has $a \approx 2$, $b \approx 1$, and $z_0 \approx 0.3$ from predictions for the obtained data [16]).

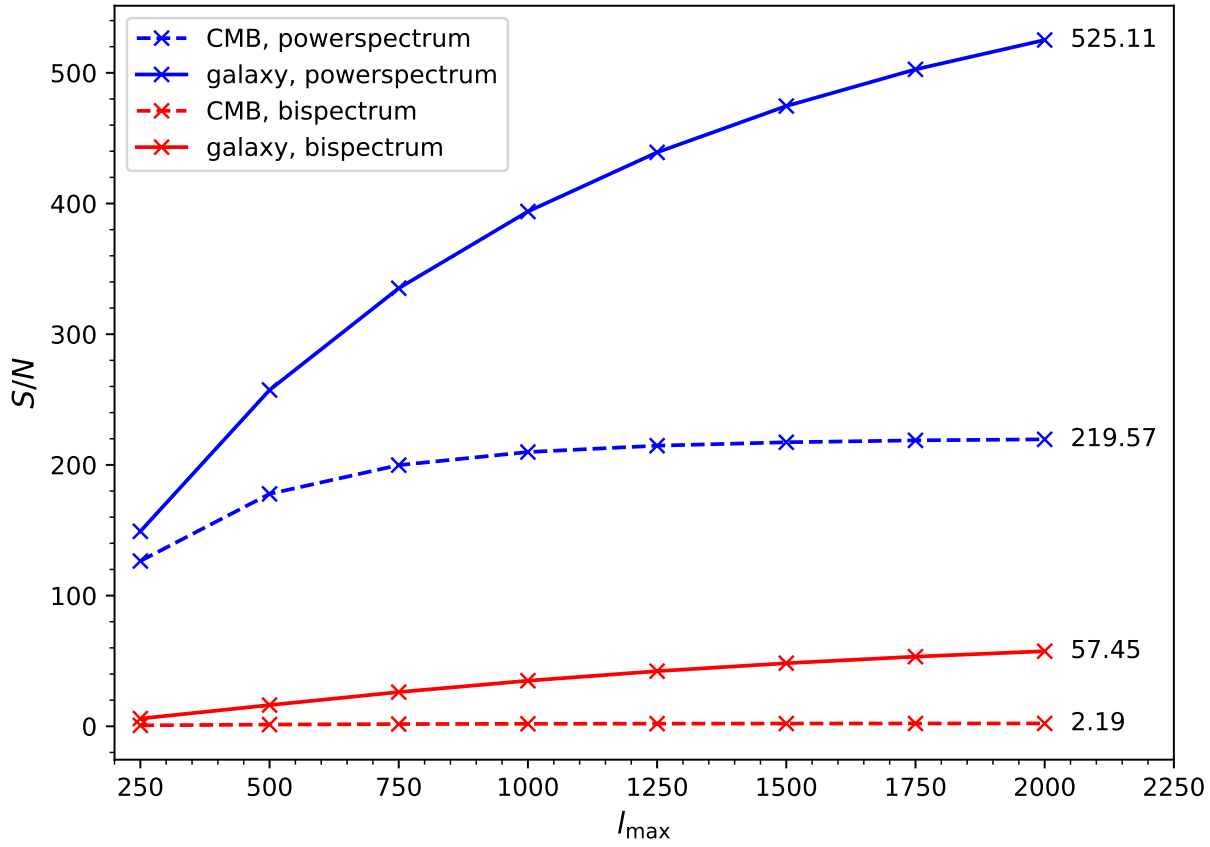

Figure 3: Signal to noise ratios for galaxy lensing (dashed) and CMB lensing (non-dashes) power- (in red) and bispectra (in blue). The x-axis labels the maximum multipole moment measured up to, starting from $l_{\min} = 50$.

5 Results

5.1 SNR

The signal to noise ratios of the CMB and galaxy lensing power- and bispectra v.s. the maximum multipole moment measured can be found in figure 3. It can be seen that the CMB bispectrum signal to noise never exceeds 2 even for $l_{\max} = 2000$, meaning that this signal is not likely to be able to contribute to parameter constraints in future surveys. All other quantities should be well detectable for $l_{\max} \geq 500$.

5.2 Parameter Constraints

For the parameter constraints, even when combining all signals, most of the parameters are poorly constrained (with minimum uncertainties much bigger than their fiducial values). The combination that is well constrained is H_0 and σ_8. Alternatively one can also look at H_0 and S_8, where S_8 is

defined as

$$S_8 = \sigma_8 \sqrt{\frac{\Omega_c + \Omega_b}{0.3}}$$

and is commonly found to be a particularly well constrained parameter in weak lensing surveys. The results are essentially the same so we will stick with σ_8. The constraints and covariances are shown in figures 4 (a) and (b). In particular, you can see in the off diagonal plot that combining the CMB and galaxy lensing removes approximate degeneracies in H_0, σ_8 space to create a much smaller 1σ confidence ellipse. When comparing powerspectra to bispectra constraints in figure 4b we see a more mild improvement in constraints when combining the different sources of information.

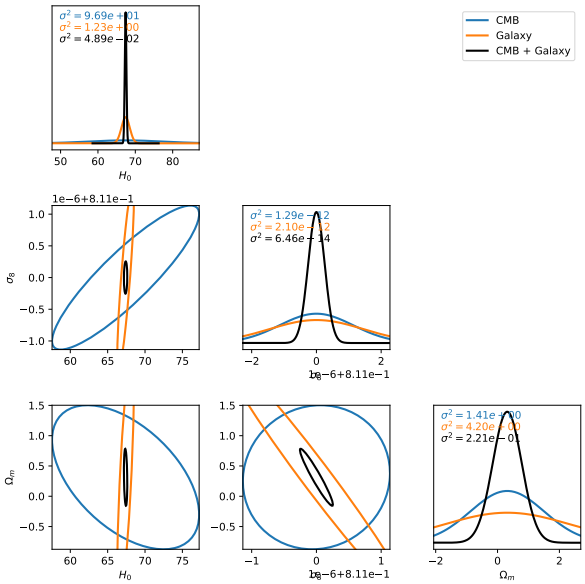

(a) Constraints for H_0 and σ_8 for CMB lensing, galaxy lensing, and CMB + galaxy lensing combined. We use the information from both power and bispectra together with $l_{\max} = 2000$ in all three cases. The confidence ellipses are for 1σ ($\sim 70\%$) certainty.

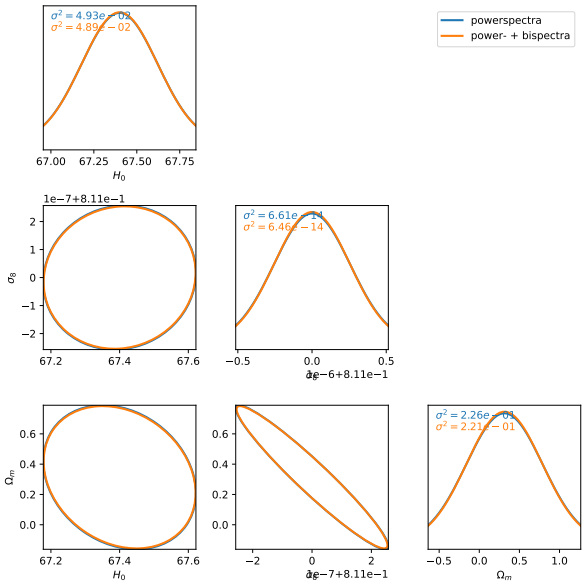

(b) Same as Fig. 4a, except comparing constraints from only using power spectra, only bispectra, or both. S_8 instead of σ_8. In all three cases we use CMB *and* galaxy lensing.

Figure 4: Side-by-side comparison of parameter constraints.

6 Discussion and conclusion

References

[1] PAR Ade, J Aguirre, Z Ahmed, et al. "The Simons Observatory: science goals and forecasts". In: *Journal of Cosmology and Astroparticle Physics* 2019.02 (2019), p. 056.

[2] N. Aghanim et al. "Planck2018 results: VI. Cosmological parameters". In: *Astronomy and Astrophysics* 641 (Sept. 2020), A6. ISSN: 1432-0746. DOI: 10.1051/0004-6361/201833910. URL: http://dx.doi.org/10.1051/0004-6361/201833910.

[3] D. Bacon, A. Refregier, and R. Ellis. "Detection of weak gravitational lensing by large-scale structure". In: *Monthly Notices of the Royal Astronomical Society* 318 (2000), pp. 625–640.

[4] Matthias Bartelmann and Peter Schneider. "Weak Gravitational Lensing". In: *Physics Reports* 340.4-5 (2001), pp. 291–472. DOI: 10.1016/S0370-1573(00)00082-X.

[5] Matthias Bartelmann and Peter Schneider. "Weak gravitational lensing". In: *Physics Reports* 340 (2001), pp. 291–472.

[6] F. Bernardeau, L. Van Waerbeke, and Y. Mellier. "Weak lensing statistics as a probe of non-Gaussian initial conditions". In: *Astronomy & Astrophysics* 322 (1997), pp. 1–18.

[7] George Casella and Roger L. Berger. *Statistical Inference*. 2nd. Duxbury Pacific Grove, CA, 2002. ISBN: 9780534243128.

[8] C. Chang et al. "The effective number density of galaxies for weak lensing measurements in the LSST project". In: *Monthly Notices of the Royal Astronomical Society* 434.3 (2013), pp. 2121–2135. DOI: 10.1093/mnras/stt1156. URL: https://academic.oup.com/mnras/article/434/3/2121/1033585.

[9] LSST Science Collaboration. *LSST Science Book, Version 2.0*. Accessed: 2025-02-11. 2009. URL: https://www.lsst.org/sites/default/files/docs/sciencebook/SB_14.pdf.

[10] Euclid Collaboration: G. Desprez, S. Paltani, J. Coupon, et al. "Euclid Preparation - X. The Euclid Photometric-Redshift Challenge". In: *Astronomy and Astrophysics* 644 (2020), A31. DOI: 10.1051/0004-6361/202039403. URL: https://www.aanda.org/articles/aa/pdf/2020/12/aa39403-20.pdf.

[11] Scott Dodelson and Fabian Schmidt. *Modern Cosmology*. 2nd. Elsevier, 2020. ISBN: 978-0-12-815948-4.

[12] Hector Gil-Marin et al. "An improved fitting formula for the dark matter bispectrum". In: *Journal of Cosmology and Astroparticle Physics* 2012.02 (2012), p. 047. DOI: 10.1088/1475-7516/2012/02/047. arXiv: 1111.4477 [astro-ph.CO].

[13] Henk Hoekstra and Bhuvnesh Jain. "Weak Gravitational Lensing and Its Cosmological Applications". In: *Annual Review of Nuclear and Particle Science* 58.1 (2008), pp. 99–123.

[14] Roger A. Horn and Charles R. Johnson. *Matrix Analysis*. 2nd. Cambridge University Press, 2012. ISBN: 978-0-521-83940-2.

[15] Ž. Ivezić, S. M. Kahn, J. A. Tyson, et al. "LSST: From Science Drivers to Reference Design and Anticipated Data Products". In: *The Astrophysical Journal* 873.2 (2019), p. 111.

[16] Steven M. Kahn, Justin R. Bankert, Srinivasan Chandrasekharan, et al. "LSST System Performance". In: *LSST Science Book, Version 2.0*. Accessed: 2025-02-11. 2009. URL: https://www.lsst.org/sites/default/files/docs/sciencebook/SB_3.pdf.

[17] N. Kaiser, G. Wilson, and G. Luppino. "Large-Scale Cosmic Shear Measurements". In: *arXiv preprint astro-ph/0003338* (2000).

[18] Alba Kalaja, P. Daniel Meerburg, and William R. Pimentel Guilherme L.and Coulton. "Fundamental limits on constraining primordial non-Gaussianity". In: *Journal of Cosmology and Astroparticle Physics* 2021.04 (Apr. 2021), p. 050. ISSN: 1475-7516. DOI: 10.1088/1475-7516/2021/04/050. URL: http://dx.doi.org/10.1088/1475-7516/2021/04/050.

[19] Martin Kilbinger. "Cosmology with cosmic shear observations: a review". In: *Reports on Progress in Physics* 78.8 (2015), p. 086901. DOI: 10.1088/0034-4885/78/8/086901. URL: https://arxiv.org/abs/1411.0115.

[20] R. Laureijs and others (Euclid Collaboration). *Euclid Definition Study Report*. ESA/SRE(2011)12. 2011. arXiv: 1110.3193.

[21] Antony Lewis, Anthony Challinor, and Anthony Lasenby. "Efficient computation of cosmic microwave background anisotropies in closed FRW models". In: *The Astrophysical Journal* 538 (2000), pp. 473–476.

[22] Abhishek S Maniyar et al. "Quadratic Estimators for CMB Weak Lensing". In: *arXiv preprint arXiv:2101.12193* (2021).

[23] Yannick Mellier et al. "Euclid. I. Overview of the Euclid mission". In: *Astronomy and Astrophysics* 662 (2024), A112. DOI: 10.1051/0004-6361/202243940. URL: https://pubs.euclid-ec.org/public/coordinated_release/PUBmellieretal.pdf.

[24] Masamune Oguri. *Lecture Notes on Weak Lensing*. Accessed: 2025-02-11. 2020. URL: https://oguri.github.io/lectures/2020kek/note_2020kek.pdf.

[25] Planck Collaboration. "Planck 2018 results. VIII. Gravitational lensing". In: *arXiv e-prints* (July 2018). arXiv: 1807.06210 [astro-ph.CO].

[26] R. Scaramella, J. Amiaux, Y. Mellier, et al. "Euclid preparation: I. The Euclid Wide Survey". In: *Astronomy and Astrophysics* 662 (2022), A112. DOI: 10.1051/0004-6361/202141938. URL: https://www.aanda.org/articles/aa/full_html/2022/06/aa41938-21/aa41938-21.html.

[27] M. Takada and B. Jain. "Cosmological parameters from lensing power spectrum and bispectrum tomography". In: *Monthly Notices of the Royal Astronomical Society* 340 (2003), pp. 580–608.

[28] Max Tegmark. "Cosmic Confusion: Degeneracies among Cosmological Parameters Derived from Measurements of Microwave Background Anisotropies". In: *Monthly Notices of the Royal Astronomical Society* 294.2 (1997), pp. 337–348. DOI: 10.1093/mnras/294.2.337.

[29] Lloyd N. Trefethen and David Bau III. *Numerical Linear Algebra*. SIAM, 1997. ISBN: 978-0-89871-361-9.

[30] L. Van Waerbeke, Y. Mellier, T. Erben, et al. "Detection of correlated galaxy ellipticities from CFH12k VLT data: first evidence for gravitational lensing by large-scale structures". In: *Astronomy & Astrophysics* 358 (2000), pp. 30–44.

[31] L. van Waerbeke et al. "Measurement of cosmic shear three-point correlations in the VIRMOS-Descart survey". In: *Astronomy and Astrophysics* 393 (2002), pp. 369–381. arXiv: astro-ph/0101511 [astro-ph].

A Fisher Matrix Analysis

A.1 Determing uncertainty in experimental parameters

Fisher matrix formalism is used to find a lower bound on the constraints we can place on experimental parameters. It combines the Cramer-Rao Inequality [7] with the assumption that we have unbiased estimators following a gaussian distribution [11]. In particular, denoting the Fisher matrix by F and the parameters as θ_i, it can be shown that

$$Var_{\theta_i}(\hat{\theta}_i) \geq \left(F^{-1}\right)_{\theta_i\theta_j}. \tag{55}$$

In the case of n potentially different random variables x_i, each with associated mean μ_{x_i} and error σ_{x_i}, the Fisher matrix is given as

$$F_{\theta_i\theta_j} := \sum_{p,q=1}^{n} \frac{\partial \mu_{x_p}}{\partial \theta_i}(\tilde{\theta}_k)(\mathrm{Cov}^{-1})_{x_p x_q} \frac{\partial \mu_{x_q}}{\partial \theta_j}(\tilde{\theta}_k), \tag{56}$$

where Cov is the covariance matrix associated with the random vector $(x_1, ..., x_n)$, $\mathrm{Cov}_{x_p x_q} := \mathrm{Cov}(x_p, x_q)$.

A.2 Fisher matrices for power- bispectra with multiple tracers

When considering power spectra, the definition of the Fisher matrix immediately gives

$$F_{\alpha\beta} = \sum_{l_{min} \leq l,l' \leq l_{max}} \sum_{[XY][X'Y']} \partial_\alpha C_l^{XY} \left(\mathrm{Cov}^{-1}\right)_{l,l'}^{XY,X'Y'} \partial_\beta C_{l'}^{X'Y'}.$$

Here the covariance matrix is given as

$$\mathrm{Cov}_{l,l'}^{XY,X'Y'} = \langle \hat{C}_l^{XY} \hat{C}_{l'}^{X'Y'} \rangle.$$

The estimator of a power or bispectrum is just the product of the estimators of the appropriate tracers, $\hat{C}_l^{XY} = \hat{X}(l)\hat{Y}(l)$. The sum over $[XY]$ and $[X'Y']$ denotes a sum over possible tracer combinations *without* counting permutations of tracer configuration. This is because permutations are not distinct signals, i.e. $\hat{X}(l)\hat{Y}(l) = \hat{Y}(l)\hat{X}(l)$. In fact, if we were to count these permutations as distinct signals we will get identical columns and/or rows in our covariance matrix making inversion impossible:

$$\langle \hat{X}(l)\hat{Y}(l)\hat{X}'(l')\hat{Y}'(l') \rangle = \langle \hat{Y}(l)\hat{X}(l)\hat{X}'(l')\hat{Y}'(l') \rangle, \quad \forall X', Y', l'.$$

To evaluate the covariance matrix we again assume that the estimators are gaussian distributed so that we can do apply a wick contraction, as is commonly done [28]. In this case we get

$$\mathrm{Cov}_{l,l'}^{XY,X'Y'} = \delta_{ll'} \left(C_l^{XX'} C_l^{YY'} + C_l^{XY'} C_l^{YX'} \right).$$

Under the Gaussian approximation the gaussian matrix thus vanishes except for 3×3 block matrices (in the case of 2 tracers) on the diagonal. The fisher matrix is then

$$F_{\alpha\beta} = \sum_{l} \sum_{[XY][X'Y']} \partial_\alpha C_l^{XY} \left(\mathrm{Cov}_l^{-1}\right)^{XY,X'Y'} \partial_\beta C_l^{X'Y'}.$$

Cov_l^{-1} here denotes the inverse of the block matrix at l.

Next, we consider the Fisher matrix for bispectra measurements.

$$F_{\alpha\beta} = \sum_{\text{distinct signals}} \sum_{\text{distinct signals prime}} B_{l_1 l_2 l_3}^{XYZ} \left(\mathrm{Cov}^{-1}\right)_{l_1 l_2 l_3, l_1' l_2' l_3'}^{XYZ,X'Z'Y'} B_{l_1' l_2' l_3'}^{X'Y'Z'}.$$

Counting only distinct signals requires more care compared to the power spectra. The rule is that $B_{l_1 l_2 l_3}^{XYZ}$ and $B_{l_1' l_2' l_3'}^{X'Y'Z'}$ are not distinct signals if there exists a permutation σ that simultaniously maps

$X'Y'Z'$ to XYZ and $l_1'l_2'l_3'$ to $l_1l_2l_3$. It turns out that we can write a sum over distinct signals out as

$$\sum_{\text{distinct signals}} = \underbrace{\sum_{l_1=l_2=l_3}\sum_{[XYZ]}}_{\text{sum 1}} + \underbrace{\sum_{l_1=l_2\neq l_3}\sum_{[XY]Z}}_{\text{sum 2}} + \underbrace{\sum_{l_1<l_2<l_3}\sum_{XYZ}}_{\text{sum 3}}.$$

With the same definition again for the $[\cdot]$ notation. For example:

$$\{[XY]Z|X,Y,Z\in\{\psi_\kappa,\psi_\gamma\}\} = \{\psi_\kappa\psi_\kappa\psi_\kappa, \psi_\kappa\psi_\gamma\psi_\kappa, \psi_\gamma\psi_\gamma\psi_\kappa, \psi_\kappa\psi_\kappa\psi_\gamma, \psi_\kappa\psi_\gamma\psi_\gamma, \psi_\gamma\psi_\gamma\psi_\gamma\}.$$

It follows to show that the sets that these sums sum over form a partition of the set of all distinct signals. Clearly all 3 sets are pairwise disjoint (no common elements) because of the criteria for the l_i's. To show that their union covers the set of distinct signals, start by considering an arbitrary signal. Its l configuration will trivially correspond to exactly one of the three sums. If it is sum 1, then we are free to permute the XYZ's by virtue of the l's being identical so we will be able to match the XYZ configuration to one of the elements of $\{\{XYZ\}\}$. Similarly, if the l configuration corresponds to sum 2, then we are free to permute the XY configuration to match with one of the elements of $\{\{XY\}Z\}$. The Z value does not matter because any Z value is accounted for. For sum 3 we can argue that we can switch around the order of the l's to satisfy $l_1 < l2 < l3$ and the corresponding XYZ configuration will be accounted for in sum 3 because all XYZ combinations are accounted. Finally, it is simple to verify that no distinct signal is counted more than once within each sum.

Covariance matrix Every element of the Fisher matrix can be seen as an inner product weighted by the inverse covariance matrix. We can choose how we order the vectors[2]. We organize the vectors according to the sum 1, 2, and 3 parts first. Then by l configuration. Within each l configuration we can choose any ordering for the XYZ configurations. The covariance matrix now becomes a block matrix with each block corresponding to a l_i and l_i' configuration. When wick contracting using the gaussian approximation, every block matrix where $l_1l_2l_3$ is not a permutation of $l_1'l_2'l_3'$ vanishes. The entries of each block matrix are given as

$$\begin{aligned}(\mathrm{Cov}_{l_1l_2l_3})^{XYZ,X'Y'Z'} = {} & C_{l_1}^{XX'}C_{l_2}^{YY'}C_{l_3}^{ZZ'} + \delta_{l_1l_2}C_{l_1}^{XY'}C_{l_2}^{YX'}C_{l_3}^{ZZ'} + \delta_{l_2l_3}C_{l_1}^{XX'}C_{l_2}^{YZ'}C_{l_3}^{ZX'} \\ & + \delta_{l_3l_1}C_{l_1}^{XZ'}C_{l_2}^{YY'}C_{l_3}^{ZX'} + \delta_{l_1l_2}\delta_{l_2l_3}\left(C_{l_1}^{XY'}C_{l_2}^{YZ'}C_{l_3}^{ZX'} + C_{l_1}^{XZ'}C_{l_2}^{YX'}C_{l_3}^{ZY'}\right).\end{aligned}$$

With our ordering this means that the covariance matrix is again a diagonal block matrix, now with blocks of size 4×4 (sum 1), 6×6 (sum 2), and 8×8 (sum 3).

A.3 Explicit form for inverse covariance matrix

The Fisher matrix above can be significantly simplified and written as

$$F_{\alpha\beta} = \sum_{l_1\leq l_2\leq l_3}\frac{\mathcal{P}_{l_1l_2l_3}}{6}\sum_{XYZ}\sum_{X'Y'Z'}\partial_\alpha B_{l_1l_2l_3}^{XYZ}(C^{-1})_{l_1}^{XX'}(C^{-1})_{l_2}^{YY'}(C^{-1})_{l_3}^{ZZ'}\partial_\beta B_{l_1l_2l_3}^{X'Y'Z'}$$

[2]The entries are the derivatives of the bispectra

where

$$C_l := \begin{pmatrix} C_l^{\psi_\kappa\psi_\kappa} & C_l^{\psi_\kappa\psi_\gamma} \\ C_l^{\psi_\kappa\psi_\gamma} & C_l^{\psi_\gamma\psi_\gamma} \end{pmatrix}$$

and $\mathcal{P}_{l_1l_2l_3}$ is defined as the number of distinct permutations that can be made with $l_1l_2l_3$. This form was, for example, used in [18][3].

To show that the above is the same as the formula for the Fisher matrix given earlier, first parition the sum in the same way and collect all terms that fit in the different categories.

$$\begin{aligned} F_{\alpha\beta} = &\sum_{l_1=l_2=l_3} \sum_{[XYZ]} \sum_{[X'Y'Z']} \partial_\alpha B^{XYZ}_{l_1l_2l_3} \left(\frac{\mathcal{P}_{l_1l_2l_3}}{6} \sum_{d.p.XYZ} \sum_{d.p.X'Y'Z'} (C^{-1})^{XX'}_{l_1} (C^{-1})^{YY'}_{l_2} (C^{-1})^{ZZ'}_{l_3} \right) \partial_\beta B^{X'Y'Z'}_{l_1l_2l_3} \\ &+ \sum_{l_1=l_2\neq l_3} \sum_{[XY]Z} \sum_{[X'Y']Z'} \partial_\alpha B^{XYZ}_{l_1l_2l_3} \left(\frac{\mathcal{P}_{l_1l_2l_3}}{6} \sum_{d.p.XY} \sum_{d.p.X'Y'} (C^{-1})^{XX'}_{l_1} (C^{-1})^{YY'}_{l_2} (C^{-1})^{ZZ'}_{l_3} \right) \partial_\beta B^{X'Y'Z'}_{l_1l_2l_3} \\ &+ \sum_{l_1<l_2<l_3} \sum_{XYZ} \sum_{X'Y'Z'} \partial_\alpha B^{XYZ}_{l_1l_2l_3} (C^{-1})^{XX'}_{l_1} (C^{-1})^{YY'}_{l_2} (C^{-1})^{ZZ'}_{l_3} \partial_\beta B^{X'Y'Z'}_{l_1l_2l_3}, \end{aligned}$$

where "*d.p.*" stands for "distinct permutations". The entries above are then the entries of the inverses of the block matrices mentioned earlier. This can be checked. For example, for the $l_1 = l_2 = l_3$ sum the multiplication of block matrices corresponding to the same l_i configuration can be written as:

$$\begin{aligned} &\sum_{[X'Y'Z']} \left(\frac{\mathcal{P}_{l_1l_2l_3}}{6} \sum_{d.p.XYZ} \sum_{d.p.X'Y'Z'} (C^{-1})^{XX'}_{l} (C^{-1})^{YY'}_{l} (C^{-1})^{ZZ'}_{l} \right) \left(C_l^{X'X''} C_l^{Y'Y''} C_l^{Z'Z''} + \text{perms } X''Y''Z'' \right) \\ &= \frac{\mathcal{P}_{l_1l_2l_3}}{6} \left[\left(\sum_{d.p.XYZ} \sum_{X'Y'Z'} (C^{-1})^{XX'}_{l} (C^{-1})^{YY'}_{l} (C^{-1})^{ZZ'}_{l} \right) C_l^{X'X''} C_l^{Y'Y''} C_l^{Z'Z''} \right] + \text{perms } X''Y''Z'' \\ &= \frac{\mathcal{P}_{l_1l_2l_3}}{6} \sum_{d.p.XYZ} \delta_{XX''}\delta_{YY''}\delta_{ZZ''} + \text{perms } X''Y''Z'' = \frac{\mathcal{P}_{l_1l_2l_3}}{6} \delta_{[XYZ],[X''Y''Z'']} + \text{perms } X''Y''Z'' \\ &= \delta_{[XYZ],[X''Y''Z'']}. \end{aligned}$$

The sum over the different wick contractions will similarly cancel with the $\mathcal{P}_{l_1l_2l_3}/6$ factor for the $l_1 = l_2 \neq l_3$ sum. For the $l_1 < l_2 < l_3$ sum the proof is similar as well except no cancellation is required.

The same type of simplification can be made in the Fisher matrix for the power spectrum, though it doesn't offer any significant benefits compared to our current 3×3 block matrix form.

A.4 Signal to Noise Ratio (SNR)

To measure the overal detectability of the lensing spectra, we introduce an overal amplitude of our signal, A, with fiducial value 1 as experimental parameter and compute F_{AA}. Obviously,

[3]Note that in [18] this is based on a previous equation summing over *all* l_i (so including permutations of each configuration) which is missing a factor of 1/6.

$\partial_A \left(AB^{XYZ}_{l_1 l_2 l_3}\right)|_{A=1} = B^{XYZ}_{l_1 l_2 l_3}$, so we find

$$\left(\frac{S}{N}\right)^2 := F_{AA} = \sum_{XYZ,X'Y'Z'} \sum_{l_1 \leq l_2 \leq l_3} \frac{\mathcal{P}_{l_1 l_2 l_3}}{6} B^{XYZ}_{l_1 l_2 l_3} (C^{-1})^{XX'}_{l_1} (C^{-1})^{YY'}_{l_2} (C^{-1})^{ZZ'}_{l_3} B^{X'Y'Z'}_{l_1 l_2 l_3}.$$

The equation for the SNR of the power spectra is identical in form.

A.5 Combined Fisher Matrix

To compute the Fisher matrix of an experiment measuring both lensing power- and bispectra we are required to compute and invert the full covariance matrix. Under the Gaussian matrix this simplifies trivially. The correlation between the a power- and bispectrum estimator contains an odd (5) amount of fields and thus always vanishes. We are thus allowed to simply add the Fisher matrices of the power- and bispectra to compute the combined Fisher matrix.

A.6 Fisher Matrices and Eigenvalues

As explained earlier, inverting the Fisher matrix gives us a covariance matrix of the estimators, $\hat{\theta}_i$ of our experimental parameters. For any vector $\mathbf{v}$,

$$\mathbf{v}_j^T \mathrm{Cov}_{ij} \mathbf{v}_i = \langle (v_i \hat{\theta}_i)^2 \rangle.$$

In particular, if the covariance matrix thus has some large eigenvalue λ_L (large compared to the overal accuracy of our experiment), with eigenvector v_i, then the corresponding estimator, $v_i \hat{\theta}_i$, has a large variance and thus represents an approximate degeneracy in our parameters. Clearly, when looking at the Fisher matrix we thus instead look for the smallest eigenvalue.

If we have such an abnormally small eigenvalue we are likely to run into problems with calculating and inverting the Fisher matrix due to numerical errors. These problems are that inversion becomes unstable and that the matrix as a whole might not be PSD because the small eigenvalue was (wrongly) calculated to be negative. These problems are likely because (1) the smallest eigenvalue is sensitive to numerical errors due to being small and (2) the errors on the eigenvalues is proportial to the condition number of the matrix [14], where the condition number is the ratio between the largest and smallest eigenvalue of the matrix [29]. Specifically, for a matrix A with some perturbation ΔA, the corresponding perturbation of eigenvalue λ_i is bounded above as

$$|\Delta \lambda_i| \leq ||\Delta A|| \kappa(A)|,$$

with $\kappa(A)$ the condition number.

Before inverting a Fisher matrix, it is thus recommended to remove rows and columns corresponding to parameters that are poorly constrained by the experiment, which can be determined by checking for small eigenvalues and their eigenvectors.

B Shear equals twice spin raised lensing potential

Consider a point on S^2, (r_0, θ_0, ϕ_0), at which we observe some cosmological object. We can then define a set of cartesian coordinates $(\tilde{r}, \tilde{y}, \tilde{x})$ as shown in figure 5.

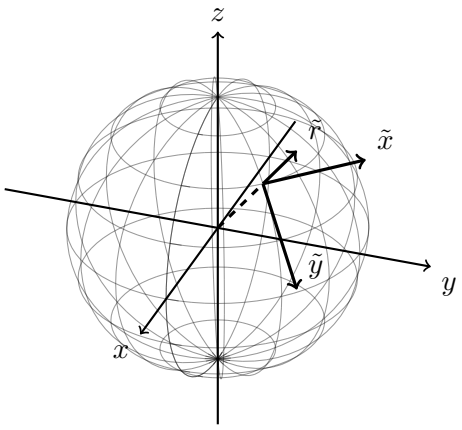

Figure 5: $(\tilde{r}, \tilde{y}, \tilde{x})$ coordinates defined for a point on the unit sphere. These act as ordinary cartesian coordinates but rotated such that, at the associated point on S^2, $\hat{\tilde{r}}$ points straight out of the unit sphere, $\hat{\tilde{y}}$ is parallel to the great arc with constant ϕ and $\hat{\tilde{x}}$ is parallel to the great arc with constant θ. These coordinates are used to define the shear and convergence in terms of the lensing potential.

Note that there it isn't obvious whether to define these coordinates at the point where the lensed light hits S^2 or the unlensed light hits S^2. We will assume that lensing effects are sufficiently weak that either definition works. We can then express the tilde coordinates in terms of spherical coordinates either by applying a rotation matrix or by calculating the r, θ, ϕ derivatives of (x, y, z) coordinates at (r_0, θ_0, ϕ_0) to find $\hat{\tilde{\mathbf{r}}}$, $\hat{\tilde{\boldsymbol{\theta}}}$, and $\hat{\tilde{\boldsymbol{\phi}}}$ and then take inner products. Regardless, we find

$$\tilde{r} = r\sin\theta\cos\phi\sin\theta_0\cos\phi_0 + r\sin\theta\sin\phi\sin\theta_0\sin\phi_0 + r\cos\theta\cos\theta_0, \tag{57}$$

$$\tilde{y} = r\sin\theta\cos\phi\cos\theta_0\cos\phi_0 + r\sin\theta\sin\phi\cos\theta_0\sin\phi_0 - r\cos\theta\sin\theta_0, \tag{58}$$

$$\tilde{x} = -r\sin\theta\cos\phi\sin\phi_0 + r\sin\theta\sin\phi\cos\phi_0. \tag{59}$$

This gives derivatives

$$\begin{aligned}
\frac{\partial}{\partial\theta} =& \left(r\cos\theta\cos\phi\sin\theta_0\cos\phi_0 + r\cos\theta\sin\phi\sin\theta_0\sin\phi_0 - r\sin\theta\cos\theta_0\right)\frac{\partial}{\partial\tilde{r}} \\
&+ \left(r\cos\theta\cos\phi\cos\theta_0\cos\phi_0 + r\cos\theta\sin\phi\cos\theta_0\sin\phi_0 + r\sin\theta\sin\theta_0\right)\frac{\partial}{\partial\tilde{y}} \\
&+ \left(-r\cos\theta\cos\phi\sin\phi_0 + r\cos\theta\sin\phi\cos\phi_0\right)\frac{\partial}{\partial\tilde{x}}. \\
\frac{\partial}{\partial\phi} =& \left(-r\sin\theta\sin\phi\sin\theta_0\cos\phi_0 + r\sin\theta\cos\phi\sin\theta_0\sin\phi_0\right)\frac{\partial}{\partial\tilde{r}} \\
&+ \left(-r\sin\theta\sin\phi\cos\theta_0\cos\phi_0 + r\sin\theta\cos\phi\cos\theta_0\sin\phi_0\right)\frac{\partial}{\partial\tilde{y}} \\
&+ \left(r\sin\theta\sin\phi\sin\phi_0 + r\sin\theta\cos\phi\cos\phi_0\right)\frac{\partial}{\partial\tilde{x}}.
\end{aligned}$$

Evaluated at our point of interest we obtain $\partial_\theta = \partial_{\tilde{y}}$ and $\partial_\phi = \sin\theta_0 \partial_{\tilde{x}}$. The second order derivatives can then be obtained using the first order derivatives. We can immediately evaluate them at the point to get

$$\begin{aligned}
\partial_\phi^2|_{(r_0,\theta_0,\phi_0)} &= -\sin^2\theta_0 \partial_{\tilde{r}} - \sin\theta_0\cos\theta_0\partial_{\tilde{y}} + \sin^2\theta_0\partial_{\tilde{x}}^2, \\
\partial_\theta\partial_\phi|_{(r_0,\theta_0,\phi_0)} &= \cos\theta_0\partial_{\tilde{x}} + \sin\theta_0\partial_{\tilde{x}}\partial_{\tilde{y}}, \\
\partial_\theta^2|_{(r_0,\theta_0,\phi_0)} &= -\partial_{\tilde{r}} + \partial_{\tilde{y}}^2.
\end{aligned}$$

Thus, at (r_0, θ_0, ϕ_0),

$$\begin{aligned}
\frac{1}{2}\eth_1(\eth_0\psi) &= \frac{1}{2}\sin\theta(\partial_\theta + \frac{i}{\sin\theta}\partial_\phi)(\frac{1}{\sin\theta}(\partial_\theta + \frac{1}{\sin\theta}\partial_\phi)) \\
&= \frac{\partial^2\psi}{\partial\theta^2} - \frac{\cos\theta}{\sin\theta}\frac{\partial\psi}{\partial\theta} + \frac{2i}{\sin\theta}\frac{\partial^2\psi}{\partial\theta\partial\phi} - \frac{1}{\sin^2\theta}\frac{\partial^2\psi}{\partial\phi^2} - 2i\frac{\cos\theta}{\sin^2\theta}\frac{\partial\psi}{\partial\phi} \\
&= \frac{1}{2}(\partial_{\tilde{y}}^2 - \partial_{\tilde{x}}^2 + 2i\partial_{\tilde{x}}\partial_{\tilde{y}})\psi = \gamma_1 + i\gamma_2 = \gamma,
\end{aligned}$$

as required.